Accepted Manuscript

Title: High-resolution turbulent flow chromatography

Author: Fabrice Gritti

PII: S0021-9673(18)30943-9
DOI: https://doi.org/doi:10.1016/j.chroma.2018.07.059
Reference: CHROMA 359571

To appear in: *Journal of Chromatography A*

Received date: 4-6-2018
Revised date: 20-7-2018
Accepted date: 24-7-2018

Please cite this article as: Fabrice Gritti, High-resolution turbulent flow chromatography, *<![CDATA[Journal of Chromatography A]]>* (2018), https://doi.org/10.1016/j.chroma.2018.07.059

Dispersion in turbulent flow of carbon dioxide is studied under retentive conditions

Performance is still limited by the slow mass transfer in the turbulent eluent

This limitation is due to slow sample transport in the viscous and buffer layers

Column efficiency is rapidly decreasing with increasing retention factor

Practical advantage of turbulent flow chromatography is demonstrated for k'<0.2

High-resolution turbulent flow chromatography

Fabrice Gritti*

Waters Corporation, Instrument/Core Research/Fundamental

Milford, MA, 01757, USA

Abstract

The resolution power of turbulent flow chromatography using carbon dioxide as the mobile phase and coated (crosslinked methyl phenyl polysiloxane) open tube columns (OTCs) as the stationary phase was investigated under retentive conditions ($0 < \mathbf{k} < 1$). The improvement in column efficiency from a laminar to a turbulent flow regime was accurately measured for small molecules (coronene and benzo[a]anthracene). This relative increase in column performance decreased from 9 to 5, 3, and to 3 with increasing the retention factor from 0 to 0.2, 0.5, and to 1.0, respectively. Despite a four to five orders of magnitude larger sample dispersion coefficient in turbulent than in laminar flow, the mass transfer in turbulent flow chromatography is still controlled and limited by the slow sample transport across the viscous layer at the column wall. The benefit of turbulent flow chromatography is then restricted to small retention factor ($\mathbf{k} <$ 0.2). From a practical viewpoint, turbulent flow chromatography using carbon dioxide as the mobile phase and 20 m long $\times$ 180 μm i.d. $\times$ 0.2 μm film thickness OTCs provides ultra-fast (analysis time $<$ 10 s) and high-resolution (plate counts of 33,000) separations of weakly retained compounds ($\mathbf{k} \sim$0.1) at Reynolds number around 5000 (3.75 mL/min, 3000 psi back pressure).

Keywords: Turbulent flow chromatography; High-resolution chromatography; Ultra-fast separation; Open tubular column; Mass transfer resistance; Carbon dioxide mobile phase.

* Tel: 508-482-2311; Fax: 508-482-3625; E-mail: Fabrice_Gritti@waters.com

*Corresponding author: (E-mail) Fabrice_Gritti@waters.com; (Tel) 508-482-2311; (Fax) 508-482-3625.

Contents

1 Introduction

It has been sixty years since Golay invented open tubular columns (OTCs) for gas chromatography (GC) analysis of complex petroleum products. At the same time, the well-known fundamental equation of band broadening in OTCs under laminar flow regime was derived : the Golay equation [1]. Aris later confirmed the exactness of this equation by applying his general dispersion theory of solute dispersion through tubes by diffusion, convection, and exchange between phases [2].

In contrast to laminar flow regime, turbulent flow along tubes occurs when the inertial stress, $\tau_{inertial} = \rho U^2$ (ρ is the fluid density and U is the linear velocity), becomes much stronger than the viscous stress, $\tau_{viscous} = \eta \frac{U}{D}$ (η is the fluid viscosity and D is the inner diameter of the tube), experienced by the fluid. However, the critical point for the onset of turbulence in pipe flow has always been a source of controversy: the critical ratio of the inertial to the viscous stress, e.g., the critical Reynolds number, typically varies over a wide range from 1500 to 3000 [3–6]. More quantitatively, the onset of turbulence has been unambigously defined and observed by experimental physicists [7]. The principle of such method consists in taking a straight pipe, applying a series of flow velocity, and in creating turbulent puffs by disturbing the inlet flow by placing a fixed obstacle at the pipe inlet. It was shown that the temporal evolution of the generated turbulent puffs determined whether the flow regime was pre-turbulent or turbulent. There are only two possible histories for the generated turbulent puffs: either they vanish or they split into two new turbulent puffs. In the first case scenario, the mean lifetime of the created turbulent puffs increases super-exponentially with increasing Reynolds number and the flow regime is laminar or pre-turbulent. In the second case scenario, their mean lifetime is decreasing super-exponentially with increasing Reynolds number and a sustained turbulent flow regime is fully developed in the pipe. Accordingly, the onset of turbulence was observed for a very accurate and precise Reynolds number of 2030 $\pm$ 10.

From the basic fundamentals of chromatography, there are *a priori* three main advantages of running OTCs under a sustained turbulent flow regime : 1) The flow velocity profile across the i.d. of the OTC is more uniform under turbulent than it is under laminar flow regime (parabolic Hagen-Poiseuille profile). Indeed, the flow profile is nearly flat across the wide and fully developed

turbulent bulk layer while the viscous wall layer across which the velocity rapidly drops to zero is relatively thin. 2) The mean sample dispersion coefficient is much larger under turbulent than it is under laminar flow regime. According to the validated model of Flint and Eisenklam [8,9], dispersion coefficients of small molecules in carbon dioxide under turbulent flow regime can be at least four to five orders of magnitude larger than their bulk diffusion coefficients. Band dispersion due to the mass transfer resistance in the mobile phase should then become irrelevant. 3) Much faster analyses can be achieved.

Soon after Golay's pioneering work in laminar GC, separation scientists rapidly turned their attention towards turbulent flow gas chromatography. In the late 1960s, Giddings [10] and Pretorius [11] were the first to investigate its potential in separation science. However, experiments revealed that turbulent GC has two serious limitations: 1) Under turbulent flow regime, the pressure drop is no longer proportional to the applied velocity but it rapidly grows as the square of the velocity [12–14]. Therefore, the maximum allowable system pressure impairs users from applying large enough Reynolds numbers along efficient narrow i.d. OTCs. 2) The gain in resolution power shrinks rapidly when increasing the retention factor of the analytes. The mass transfer resistance between the mobile and stationary phase increases rapidly with increasing the retention factor **k**. Overall, the observed plate heights in turbulent gas flow (Re=5000) were five **and** two times smaller than those observed in laminar gas flow (Re=2000) **for retention factors of 0 and 1** [11,15,16], respectively.

Data on band broadening in turbulent flow chromatography using OTC and carbon dioxide as the mobile phase are very scarce. The Schmidt number, $Sc = \frac{\eta}{\rho D_m}$ (D_m is the bulk diffusion coefficient), of supercritical carbon dioxide above 304 K and at atmospheric pressure is typically around 10 for small molecules. According to Pretorius and Aris [11], the reduced plate height of OTCs is then expected to decrease from about 70 to 0.7 when increasing the Reynolds number from 2000 to 5000, a 100 times increase in column efficiency. The very first attempts were recently made under non-retained conditions using 180 μm i.d. $\times$ 5 m [17] and 20 m [14] long OTCs and carbon dioxide as the mobile phase at lab temperature and average pressures in the range from 100 to 250 bar. Irrespective of the bulk diffusion coefficient of the analyte, these data revealed that the height equivalent to a theoretical plate (HETP) decreased by about the same factor 9 when the

Reynolds number was increased from 2000 to 5000. For the sake of comparison, the extension of the classical Golay equation valid for laminar flow to a more general equation also applicable to turbulent flow was performed for velocity profiles represented by polynomials of any order $n \geq 2$ [18–20]. n is increasing with increasing the Reynolds number. The classical Golay HETP equation reduces to the general Golay HETP equation for the specific value of n=2 (parabolic flow profile) [20]. A polynomial of order n=10 is an excellent representation of the actual turbulent flow profile across the OTC at Re=4000 [21]. According to the general Golay HETP equation and to the validated Flint and Eisenklam model for turbulent dispersion, the HETP are expected to decrease by a factor as large as 250 for small molecules and D_m values around 5.0×10^{-5} cm^2/s. This large discrepancy between predictions (a factor 100 according to Pretorius and Aris, 250 according to Golay) and observations (a factor 9 only) was explained by 1) the presence of unstable and decaying turbulent puffs at $Re = 2000$ (the actual dispersion coefficient is six times as large as D_m, which is assumed to be true in the laminar Golay equation) and 2) by the finite and slow mass transfer across the viscous layer at Re=5000 (which is assumed to be infinitely fast in the general Golay HETP model because the turbulent dispersion coefficient is assumed to be uniform across the entire OTC i.d.) [14]. In order to assess the potential of high-resolution turbulent chromatography in OTCs under retentive conditions, additional data are desperately needed for retained analytes.

Therefore, in this work, the reduced plate height (RPH) of small polycyclic aromatic hydrocarbon (PAH) molecules (coronene and benzo[a]anthracene) are first accurately measured as a function of the average Reynolds number from 500 to 15000 for four different retention factors increasing from **k**=0 to 0.2, 0.5, and to 1.0. The OTC is a 180 μm i.d. $\times$ 20 m long $\times$ 0.2 μm film thickness (crossbond phenyl methyl polysiloxane) and the mobile phase is a mixture of carbon dioxide **(98% or 99% in volume)** and methanol. The OTC is placed in a temperature-controlled GC oven in order to maintain constant the retention factor within 5% when the flow rate is increased stepwise. The experimental plots of the HETP *versus* the Reynolds number are then compared to the theoretical ones and the impact of the retention factor on the gain in resolution power upon performing under turbulent relative to laminar flow conditions are measured, reported, and discussed. From a practical viewpoint, it is determined from the presented data for which experimental con-

ditions turbulent flow chromatography should become advantageous over classical chromatography in OTCs.

2 Theory

In this section, the list of equations used in this work is given without demonstration. All the details regarding the definition and derivation of these equations are given in references [14,17,20]. In particular, the determination of the average Reynolds number along the capillary column described in [14] assumed that the temperature of the OTC is uniform. Indeed, the 20 m $\times$ 180 μm OTC is placed in a GC oven which fixes the capillary temperature in a range from room temperature to 135°C. Accordingly, the adiabatic cooling of carbon dioxide at large pressure drop is irrelevant because the OTC, whose outer diameter is very thin (360 μm only), is instantaneously at thermal equilibrium with the air in the GC oven. As a result, the temperature of carbon dioxide along the capillary column can be considered as strictly uniform.

The Reynolds number Re [21] and the critical Reynolds number Re_c above which a sustained turbulent flow is established are given by [7] :

$$Re = \frac{\rho \overline{U} D}{\eta} \quad ; \quad Re_c = 2030 \pm 10 \tag{1}$$

where D is the i.d. of the OTC, ρ and η are the average density and dynamic viscosity, respectively, of the fluid along the OTC, and $\overline{U}$ is the average linear velocity along the OTC.

Irrespective of the Reynolds number, the local linear velocity, $\overline{u}(r)$, at the radial position r is represented by a polynomial of order n [17,20]:

$$\overline{u}(r) = \frac{n+2}{n}\overline{U}\left[1 - \left(\frac{2r}{D}\right)^n\right] \tag{2}$$

where $n \geq 2$ depends directly on the Reynolds number $Re > Re_c$ [17]. If $Re < Re_c$, the flow profile is parabolic and n=2 (Hagen-Poiseuille flow profile).

The pressure drop along the OTC is given from the well-known Darcy-Weibach equation [21]:

$$\Delta P = \frac{1}{2} f_D(Re) \frac{L}{D} \rho \overline{U}^2 \tag{3}$$

where L is the OTC length and $f_D(Re)$ is the friction factor, which depends only on the Reynolds

number for smooth pipes such as fused silica capillaries [17,22]. This assumption is not rigorously true for the 180 μm i.d. stainless steel tubes present in the SFC system used in this work : their inner surface is not ideally smooth with a roughness around 0.1 μm / 180 μm $\sim$ 0.0005 after electropolishing the stainless steel tubes. According to the Colebrook equation [23], the maximum error in the friction factor is smaller than a few percents for Reynolds numbers smaller than 15000. Therefore, the assumption of smooth tubes remains a good approximation for the prediction of pressure drops along the SFC system.

The general Golay HETP equation, which assumes polynomial flow velocity profiles (Eq. 2) and uniform distribution of the mean sample dispersion coefficient $\overline{D_a}$ across the whole OTC i.d., is written [18–20]:

$$h = \frac{2}{\nu}\frac{\overline{D_a}}{D_m} + \frac{1+[n+4]\mathbf{k}+[\frac{n^2}{4}+\frac{5}{2}n+5]\mathbf{k}^2}{4(n+2)(n+4)(1+\mathbf{k})^2}\frac{D_m}{\overline{D_a}}\nu + \frac{2}{3}\frac{\mathbf{k}}{(1+\mathbf{k})^2}\frac{D_m}{D_s}\left[\frac{d_f}{D}\right]^2\nu \tag{4}$$

where $\nu = \frac{\overline{U}D}{D_m}$ is the reduced linear velocity, D_m is the bulk diffusion coefficient of the analyte, n is a positive number that depends on the Reynolds number [17] (n is increasing with increasing Re), $\mathbf{k}$ is the retention factor of the analyte, D_s is the bulk diffusion coefficient of the analyte in the stationary film ($D_s \sim 5 \times 10^{-7}$ cm^2/s [24] in crosslinked polysiloxane), and d_f is the thickness of the coated stationary film (d_f=0.2 μm).

In the general Golay HETP equation, the bulk diffusion coefficient D_m was estimated from the Wilke & Chang equation [14,25], $\overline{D_a}$ is given by Eqs 6 and 7 in reference [14], $\frac{D_m}{D_s}$=100 [24], , and $\mathbf{k}$ is given in this work by:

$$\mathbf{k} = \frac{t_R - t_{R,ACN}}{t_{R,ACN}} \tag{5}$$

where t_R and $t_{R,ACN}$ are the observed elution times of the PAH analytes (coronene or benzo[a]anthracene) and of the non-retained sample diluent (acetonitrile), respectively.

Writing that diffusive and convective fluxes are additive, $\overline{D_a}$ is written:

$$\overline{D_a} = D_m + \overline{D_t} \tag{6}$$

where $\overline{D_t}$ is the average turbulent dispersion coefficient over the entire i.d. of the OTC [8,14]. Accordingly, $\overline{D_t}$ is four to five orders of magnitude larger than D_m ($\sim 5 \times 10^{-5}$ cm^2/s) at a Reynolds number in the range from 5000 to 15000.

In contrast to the assumption made for the derivation of the general Golay HETP equation, Quarmby et al. [26] have observed that the local intensity of $\overline{D_a}$ across the i.d. of the OTC was in fact best described by:

$$D_a(x) = D_m + \frac{10}{9}\overline{D_t}(1 + 3x^2 - 4x^3) \tag{7}$$

where $x = \frac{2r}{D}$ is the reduced radial coordinate.

According to Eq. 7, $D_a = D_m$ and $D_a = D_m + \frac{10}{9}\overline{D_t} \sim 1.1\overline{D_t}$ at the wall (x=1) and at the center (x=0) of the OTC, respectively. It is noteworthy that D_a is maximum for $x = 0.5$ and takes the value $D_m + \frac{25}{18}\overline{D_t} \sim 1.4\overline{D_t}$. This means that a severe gradient of the local dispersion coefficient is expected from the bulk to the wall region of the OTC.

2.1 Estimation of the bulk diffusion coefficients in carbon dioxide-methanol mixtures

The bulk diffusion coefficients of coronene and benzo[a]anthracene in their respective mobile phase were systematically estimated from the Wilke and Chang equation for all flow rates [25]:

$$D_m = 7.4 \times 10^{-8}\sqrt{x_v\phi_{CH_3OH}M_{CH_3OH} + (1 - x_v)\phi_{CO_2}M_{CO_2}}\frac{T_{lab}}{\overline{\eta}_{cap}V_b^{0.6}} \tag{8}$$

where ϕ_{CH_3OH}=1.9 and ϕ_{CO_2}=1.0 are the association factors of the solvents, M_{CH_3OH}=32 g/mol and M_{CO_2}=44 g/mol are the molecular weights of the solvents, $\overline{\eta}_{cap}$ is the average viscosity along the capillary column, and V_b is the molar volume of the pure analyte at its boiling point. V_b was estimated from the Lebas and Schroeder group/atom contribution methods for both analytes [27]. V_b is then equal to 294.0 (Schroeder) and 309.6 (Lebas) cm^3/mol for coronene and to 245.0 (Schroeder) and 250.8 (Lebas) cm^3/mol for benzo[a]anthracene. Accordingly, in the estimation of the diffusion coefficients, V_b=301.8 and 247.8 cm^3/mol for coronene and benzo[a]anthracene, respectively.

3 Experimental

3.1 Chemicals

The mobile phases used were mixtures of pure industrial carbon dioxide (99.8% pure) purchased from Airgas (Worcester, MA, USA) and methanol (volume fractions of 1% or 2%). Isopropanol was used as a post-capillary make-up solvent (0.1 mL/min) in order to avoid precipitation of the PAH analytes and clogging inside the ABPR. Two sample solutions were prepare: the coronene (0.5 g/L dissolved in dichloromethane) and benzo[a]anthracene (0.5 g/L dissolved in acetonitrile) sample solutions were stored in 2 mL vials. Both acetonitrile and dichloromethane were HPLC grade and purchased from Fisher Scientific (Fair Lawn, NJ, USA). Coronene and benzo[a]anthracene were both purchased from Sigma-Aldrich (Suwannee, GA, USA) with a minimum purity of 99%.

3.2 Instrument and materials

The ACQUITY UPC^2 system (Waters, Milford, USA) was used to record the peak profiles of acetonitrile and coronene. A complete description of this system was recently given in reference [14]. Additionally, an isocratic pump (Waters, Milford, USA) delivered pure isopropanol post-column at a constant flow rate of 0.1 mL/min in a tee union prior to the active back pressure regulator (ABPR). In order to maintain constant the retention factor, **k**, of the analyte when increasing the flow rate and the average density of the mobile phase, the temperature of the capillary column was accurately controlled by placing it in the oven of an HP 5890 GC system. The inlet of the 20 m $\times$ 180 μm fused silica glass capillary column was directly connected to the six-port injection valve in order to minimize sample dispersion due to injection. Its outlet is connected to the tee union just prior to the ABPR. A 1 μL injection loop was used. Post-column sample dispersion was reduced to zero by performing detection directly on-capillary (after burning out the 20 μm thick polyimide sleeve and meticulously cleaning the glass surface) using an optical fiber guiding the UV-Vis light directly onto the capillary wall.

3.3 Capillary column

A 180 μm i.d. $\times$ 20 m $\times$ 0.2 μm film thickness (crosslinked methyl phenyl polysiloxane) fused silica glass capillary column was purchased from Resteck (Bellafonte, PA, USA). Its outer diameter is 360 μm covered with a 20 μm thick polyimide film. The inlet end of the capillary column was modified as follows: it was first wrapped with a 2.5 cm $\times$ 360 μm **i.d.** beige PEEK tube. Then, a short metallic sleeve (2.0 cm long, 1/16" O.D.) was **first slid and then crimped** against the PEEK tube. Finally, a metallic nut and a ferrule were assembled directly in the port of the injection valve 1. The outlet end was wrapped with a 2.5 cm $\times$ 360 μm **i.d. and 1/16" o.d** orange PEEK sleeve and connected to the tee union with a plastic ferrule. On-capillary detection was performed exactly at L_{corr} =19.6 m. The capillary column was placed in the oven of the GC instrument. **Note that a fraction of the column length was kept outside the oven. The lengths of the inlet and outlet ends of the 20 m long capillary left outside the oven were about 40 cm long, respectively.**

3.4 Chromatographic experiments

In all the following experiments, the ABPR pressure was fixed at 1500 psi. **The rationale for the selection of such a low backpressure was to broaden as much as possible the range of applied flow rates in order to reach Reynolds number of at least 5000 at room temperature. The maximum system pressure is limited to 6000 psi.**

3.4.1 Coronene sample: k=0

0.4 μL of a solution of coronene (0.5 g/L in pure dichloromethane) was injected at flow rates of mixtures of carbon dioxide and methanol (premixing volume fraction x_v=1%) increasing from 0.50 to 0.75, 1.00, 1.25, 1.50, 1.75, 2.00, 2.25, 2.50, 2.75, 3.00, 3.25, 3.50, and to 3.70 mL/min. The temperature of the capillary column was imposed by the lab temperature at 296 K $\pm$ 1 K (no temperature control from the GC oven). The total system pressure increased from 1575 to 1630, 1707, 1800, 1910, 2030, 2256, 2474, 2719, 2973, 3254, 3548, 3882, and to 4158 psi. Coronene is not retained under these conditions. The peak profiles of coronene were recorded at a wavelength and

sampling rate of 200 nm and 80 Hz, respectively. The corresponding chromatograms are shown in Figure 1.

3.4.2 Benzo[a]anthracene sample: k=0.2

0.4 μL of a solution of benzo[a]anthracene (0.5 g/L in pure acetonitrile) was injected at increasing flow rates of mixtures of carbon dioxide and methanol (x_v=2%) increasing from 0.50 to 0.75, 1.00, 1.25, 1.50, 1.75, 1.88, 2.00, 2.12, 2.25, 2.50, 2.75, 3.00, 3.25, 3.50, and to 3.75 mL/min. In order to maintain the retention factor constant at k=0.2 ±0.01 upon increasing the flow rate and the average density of the mobile phase (and an inevitable decrease of the retention factor), the capillary temperatures were imposed by the GC oven at 25, 25, 25, 25, 25, 26, 26, 26, 27, 27, 28, 29, 30, 32, 34, and 37°C, respectively. The total system pressure increased from 1584 to 1651, 1741, 1840, 1961, 2088, 2212, 2332, 2449, 2579, 2851, 3126, 3435, 3765, 4118, and to 4510 psi. The peak profiles of benzo[a]anthracene were recorded at a wavelength and sampling rate of 275 nm and 80 Hz, respectively. The corresponding chromatograms are shown in Figure 2.

3.4.3 Benzo[a]anthracene sample: k=0.5

0.4 μL of a solution of benzo[a]anthracene (0.5 g/L in pure acetonitrile) was injected at increasing flow rates of mixtures of carbon dioxide and methanol (x_v=2%) increasing from 0.50 to 0.75, 1.00, 1.25, 1.50, 1.75, 1.88, 2.00, 2.12, 2.25, 2.50, 2.75, 3.00, 3.25, and to 3.50 mL/min. In order to maintain the retention factor constant at k=0.50 ±0.03, the capillary temperatures were imposed by the GC oven at 42, 43, 44, 45, 48, 50, 52, 55, 57, 59, 63, 68, 76, 85, and 96°C, respectively. The total system pressure increased from 1573 to 1648, 1732, 1850, 1980, 2337, 2472, 2605, 2750, 2915, 3264, 3660, 4115, 4638, and to 5247 psi. The peak profiles of benzo[a]anthracene were recorded at a wavelength and sampling rate of 275 nm and 80 Hz, respectively. The corresponding chromatograms are shown in Figure 3.

3.4.4 Benzo[a]anthracene sample: k=1.0

0.4 μL of a solution of benzo[a]anthracene (0.5 g/L in pure acetonitrile) was injected at increasing flow rates of mixtures of carbon dioxide and methanol (x_v=2%) increasing from 0.50 to 0.75, 1.00, 1.25, 1.50, 1.75, 1.88, 2.00, 2.12, 2.25, 2.50, 2.75, 3.00, and to 3.25 mL/min. In order to maintain the retention factor constant at k=1.00 ±0.06, the capillary temperatures were imposed by the GC oven at 48, 50, 52, 53, 55, 60, 64, 67, 70, 73, 90, 103, 118, and 135°C, respectively. The total system pressure increased from 1593 to 1671, 1746, 1882, 2017, 2384, 2602, 2750, 2908, 3100, 3691, 4148, 4693, and to 5344 psi. The peak profiles of benzo[a]anthracene were recorded at a wavelength and sampling rate of 275 nm and 80 Hz, respectively. The corresponding chromatograms are shown in Figure 4.

3.5 Plate height measurements

The first and second central moments (μ_1 and $\mu_2^{'}$) of the experimental peaks shown in Figures 1, 2, 3, and 4 were extracted from the best fit of a Gaussian function to the experimental peaks shown in Figures 4 and 5 after a linear baseline shift correction. The fitting procedure was done with the software Peakfit version 4.12 (SeaSolve Software, Inc.). The experimental reduced plate heights were then all determined from the definition of the plate height:

$$h = \frac{L_{corr}}{D_{cap}} \frac{\mu_2^{'}}{\mu_1^2} \tag{9}$$

The temporal moments were not corrected for pre-capillary column sample dispersion because the volumes of the injection loop volume (1.0 μL) and connecting tube 6 (6.0 μL) account for only 1% of the capillary volume (510 μL).

It is important to keep in mind that the non-negligible pressure drop along the isothermal column implies some significant changes in the local density, viscosity, and linear velocity of the mobile phase. In this work, this effect was averaged by measuring the density, viscosity, linear velocity, and Reynolds number from the mean values of these eluent properties (taken as the average of the inlet and outlet column values as

previously shown in details in reference [14]). The impact of the axial heterogeneity of the linear velocity along the capillary column on the apparent plate height measured from the time-based moments at the column outlet was not investigated in this work. This deserves a deeper investigation and a fundamental study on the basis of Giddings theory of non-uniform columns [15] from the exact variations of the local linear velocity along the column. This will be analyzed in depth in a forthcoming work.

3.6 Dispersion coefficient measurements

The average dispersion coefficients $\overline{D_a}$ were estimated experimentally by matching the observed RPH to general Golay HETP equation 4. It is important to recall the two main assumptions of the HETP equation : 1) the flow profile is well described by a polynomial of order n and 2) the dispersion coefficient $\overline{D_a}$ is uniform over the entire volume of the OTC.

4 Results and Discussion

4.1 Analysis of the experimental temporal peak profiles

Figures 1, 2, 3, and 4 show the experimental peak profiles of coronene (**k**=0) and benzo[a]anthracene (**k**=0.2, 0.5, and 1.0) as a function of the applied flow rate. Importantly, the OTC temperature was adjusted (increased) stepwise in order to maintain the retention factor of benzo[a]anthracene constant when increasing stepwise the flow rate. That is because the increase of the flow rate of the mobile phase (carbon dioxide/methanol mixture) leads to an increase of its average density along the OTC and, therefore, to a diminution of the retention factor. This drop in retention was corrected by a slight increase of the GC oven temperature. The outer diameter of the OTC is very small (360 mum), so, it takes no more than a few seconds before the column reaches thermal equilibrium with the GC oven. Maintaining the retention factor constant was critical because the mass transfer resistance in the mobile phase across the i.d. of the OTC is strongly dependent on **k**, at least under laminar flow regime as described by the Golay equation [1,2]. By precaution, irrespective of the applied flow rate and under sustained turbulent flow regime, it was made sure that the retention factor of benzo[a]anthracene remained constant within ± 5%.

The most striking experimental information from Figures 1 to 4 is that the transition from a laminar to a sustained turbulent flow regime is directly revealed from the evolution of the peak height (for a constant injection volume) as a function of the flow rate imposed. In theory, the peak height should decrease continuously if a laminar flow regime would persist over the entire range of applied **velocities**. Clearly, this is experimentally not the case: a sudden increase of the peak height is unambiguously observed beyond a particular flow rate (1.75 mL/min for **k**=0 and 0.2, 1.50 mL/min for **k**=0.5 and 1.0). This inevitably indicates a change in the nature of the mass transfer mechanism along the OTC. This change is directly related to the transition from a pre-turbulent to a sustained turbulent flow regime. However, the data shown in Figures 1 to 4 reveal that it is not possible to determine accurately the critical Reynolds number (Re_c=2030) or the precise onset of turbulence from simple band spreading data by chromatography. Only physico-chemical data pertaining to the observation of decaying and/or splitting turbulent puffs in pipe flow [7] enables its

accurate determination. Roughly, the estimated critical flow rates above which the nature of the mass transfer mechanism in the OTC is changed are observed at 1.75, 1.75, 1.50, and 1.50 mL/min for retention factors **k** of 0, 0.2, 0.5, and 1.0, respectively. Accordingly, the corresponding critical Reynolds number are measured at 2360, 2290, 3586, and 3631, respectively. This demonstrates that the sudden increase in peak height is not a good indicator for the onset of turbulence in pipe flow. Interestingly, the sudden increase in the height of the chromatographic peak always provide an overestimated value of the true critical Reynolds number. The reason for this observation is given in the next section where the plots of the RPH *versus* the reduced velocity are analyzed in depth.

4.2 Analysis of the RPH plots

Figures 5, 6, 7, and 8 show the corresponding experimental RPHs of coronene (**k**=0) and benzo[a]anthracene (**k**=0.2, 0.5, and 1.0) as a function of the measured Reynolds number. The accurate measurement of the average Reynolds number along the OTC has been previously described in a previous work [14].

4.2.1 Onset of turbulence

Interestingly, irrespective of the retention factor, these RPH *versus* Re plots (empty green stars) show evidence that the RPH starts diminishing when the Reynolds number has already exceeded 2030. Therefore, the reduction of the RPH is not observed at the true critical Reynolds number Re_c=2030. This is directly explained by the presence of randomly formed, unstable and decaying turbulent puffs in carbon dioxide even under a pre-turbulent flow regime. Consistent with this explanation, for Re <2000, the experimental RPHs are well smaller than the predicted ones (full red circles, classical Golay equation), which assume that the dispersion coefficient is equal to the bulk diffusion coefficient D_m. Additionally, the extrapolation of the turbulent experimental RPH data to lower Reynolds numbers (see the dashed green line in Figures 5, 6, 7, and 8) intersects the laminar Golay RPH plot (full red circles) at a Reynolds number which is very close to the true critical Reynolds number of 2030. In conclusion, the onset of turbulence revealed by chromatographic

measurements is somewhat delayed relative to the true occurrence of the transition from laminar to turbulent flow.

4.2.2 Mass transfer resistance in the stationary phase

It is noteworthy that the mass transfer resistance in the stationary film accounts for less than 10% of the total experimental RPH (see the purple empty circles in Figures 6, 7, and 8 for $\mathbf{k} \neq 0$). Its contribution is small because the selected thickness of the crosslinked polymethylphenylsiloxane film was purposefully kept very thin at 0.2 μm only. At the highest applied flow rates, its relative contribution decreases from 7% to 3% and to 2% when increasing the retention factor from 0.2 to 0.5 and to 0.5, respectively. To summarize, the slow diffusivity ($\sim 5 \times 10^{-7}$ cm^2/s) of the sample in the stationary film has no significant impact on the observed peak width and HETP.

4.2.3 Longitudinal dispersion

Longitudinal dispersion is always negligible in laminar flow regime because the reduced velocities applied are very large in the range from about 10000 to 100,000. Even in the presence of unstable turbulent puffs in a laminar flow regime ($\frac{\overline{D_a}}{D_m} \sim 6$ [14]), the term $\frac{2}{\nu}\frac{\overline{D_a}}{D_m}$ in the general Golay HETP equation 4 is always negligible relative to the total observed RPH.

In contrast, in turbulent flow regime, this contribution becomes much more important because the dispersion coefficient $\overline{D_a}$ is four to five orders of magnitude larger than D_m [14]. Figures 9, 10, 11, and 12 plot the values of $\overline{D_a}$ as a function of the Reynolds number (full blue stars) according to the Flint model of turbulent dispersion [8]. Accordingly, the turbulent dispersion coefficient of any analyte is about constant at 3-4 cm^2/s in the range of Reynolds number from 2500 to 15000. Consequently, at Re=2500 and 5000, the RPH term related to longitudinal dispersion (first RPH term in the right-hand-side of Eq. 4) along the OTC is equal to 3.5 and 1.3, respectively. As the retention factor increases from 0 to 0.2, 0.5, and to 1.0, the average relative contribution of this RPH term to the total observed RPH decreases rapidly from about 33% to 5%, 1%, and to 0.5%, respectively. Longitudinal dispersion is then only relevant under non-retained or weakly retained conditions. It is definitely negligible for $\mathbf{k}$ larger than 0.5. This means that the observed mass

transfer along the OTC is still governed by the slow mass transfer in the turbulent mobile phase. The large contribution of the mass transfer resistance in the mobile phase to the total observed RPH is analyzed in the next section.

4.2.4 Mass transfer resistance in the mobile phase

Remarkably, the RPHs measured under sustained turbulent flow are increasing with increasing the retention factor. For instance, at Re=4000, the RPH is increasing from 6 to 30, 80, and to 150 with increasing the retention factor from 0 to 0.2, 0.5, and to 1.0, respectively. In contrast, the turbulent Golay RPH plot (empty blue circles), which assumes that the dispersion coefficient $\overline{D_a}$ is strictly uniform over the entire volume of the OTC, is weakly affected by the retention factor $\mathbf{k}$: the predicted RPHs are much smaller as they increases from 1.3 to 2.3, 2.6, and to 3.1, respectively. This increase is also partly due to the larger RPH term associated to the slow mass transfer in the stationary film (see the purple empty circles in Figures 6, 7, and 8 for $\mathbf{k} \neq 0$). Therefore, the large discrepancy (about one order of magnitude) between the experimental and the theoretical RPHs are explained by either a wrong prediction of the dispersion coefficient $\overline{D_a}$ (Flint model [8]) and/or the non-applicability of the turbulent Golay model. Because the Flint model of turbulent dispersion has been validated experimentally from several independent series of data ([9,28,29]), the turbulent Golay model is necessarily inapplicable and suffers from a wrong assumption: the dispersion coefficient D_a is not uniform across the entire i.d. of the OTC because the turbulent flow regime is not fully developed in the viscous layer (where the flow velocity is fully controlled by viscous forces) and in the buffer layer (where the viscous forces are still dominating the inertial forces) both located in the wall region of the OTC.

For the sake of illustration, the radial distribution of the dispersion coefficient has been measured in turbulent gas flow (Schmidt number Sc=0.77) for Reynolds number in the range from 21000 to 130000 [26] (see Figure 13): irrespective of the Reynolds number, it is best represented by Eq. 7 with a minimum at the wall ($D_a = D_m$), a maximum ($D_a \sim 1.4\overline{D_t}$) at half the distance between the center and the wall of the OTC, and an intermediate value in the very center of the OTC ($D_a \sim 1.1\overline{D_t}$). Consequently, the turbulent Golay model cannot predict accurately the RPH associated to the mass

transfer resistance in the mobile phase across the i.d. of the OTC. For instance, at a Reynolds number of 4000, the second RPH term in the right-hand-side of Eq. 4 increases from 0.002 to 0.006, 0.017 and to only 0.033 when increasing the retention factor from 0 to 0.2, 0.5, and to 1.0, respectively. In fact, the observed RPH associated to the slow mass transfer in the mobile phase increases from 3.6 to 27, 85, and to 165, respectively. The general Golay HETP model is then strongly underestimating this RPH term by one to two orders of magnitude.

4.2.5 Overall performance

Unlike the predictions of the general Golay HETP equation, the previous analysis of the experimental variations of the different RPH terms (slow diffusion in the stationary phase, longitudinal dispersion, mass transfer resistance in the mobile phase) has revealed that the overall band broadening mechanism along the OTC under a sustained turbulent flow remains controlled by the slow mass transfer in the carbon dioxide mobile phase. This is especially true when applying large retention factors. As a result, as shown in Figures 5, 6, 7, and 8, the total RPH of the OTC is reduced by a factor 9, 5, 3, and 3 when the Reynolds number is increasing from 2300 to 5000 for retention factors of 0, 0.2, 0.5, and 1.0, respectively. These data clearly reveal that 1) the RPH increases and 2) the relative gain in column performance from laminar to turbulent flow is diminished by a factor three when increasing the retention factor in a range from 0 to 1. The practical interest of turbulent flow chromatography is obviously to perform separations for the lowest sample retention factors.

4.3 Practical considerations

4.3.1 Peak capacity

The peak capacity expected in turbulent flow chromatography using open tubes can now be estimated based on the variation of the reduced plate height with increasing the retention factor. The general definition of the peak capacity based on a 4σ baseline

peak width is:

$$P_c = 1 + \int_{t_0}^{t_L} \frac{dt}{4\sigma(t)} \tag{10}$$

where t_0 is the hold-up time of the column, t_L is the arbitrary retention time of the last eluted compound, and $\sigma(t)$ is the temporal standard deviation of the concentration distribution of the analyte eluting at the time t.

Changing the variable time (t) to the variable retention factor (k), Eq. 10 becomes under isocratic conditions:

$$P_c = 1 + \int_{0}^{k_L} \frac{1}{4}\sqrt{\frac{L}{d_c}} \frac{dk}{(1+k)\sqrt{h(k)}} \tag{11}$$

where k_L is the retention factor of the last eluted compound and $h(k)$ is the expression of the reduced plate height of the open tube as a function of the retention factor.

For the sake of application, let us consider k_L=1, L=20 m, and d_c=180 μm. Based on the previous sections, it is observed that $h(0)$=5, $h(0.2)$=25, $h(0.2)$=70, and $h(1)$=100. Accordingly, the variation of the expected peak capacity when increasing the retention factor of the last eluted compound from k=0 to k=1 is represented in Figure 14. Interestingly, a maximum of five and ten compounds can be baseline separated for k_L=0.2 and 1.0, respectively. Applications of turbulent flow chromatography in open tubes is then definitely limited to simple complex mixtures such as enantiomers or the identification of unknown impurities co-eluting with a main peak. This will be illustrated in the next section.

4.3.2 Potential Application

Based on the previous observations on the mass transfer mechanism of small molecules along OTC from laminar to turbulent flow regimes, the possible application in separation science of carbon dioxide/organic solvent mixtures as turbulent mobile phases is necessarily limited to small retention factors (**k** <0.2) and to simple sample mixtures containing at most a few compounds. Otherwise, the gain in chromatographic performance would not be significant given the price in pressure that has to be paid [14].

Accordingly, the advantage of turbulent flow chromatography along 180 μm $\times$ 20 m coated (0.2 μm thick film) OTCs was demonstrated for the separation of an unknown impurity present in the sample coronene. A carbon dioxide/methanol (99/1, v/v) mobile phase was used at room temperature (296 K) in the experiments. The results are presented in Figure 15 at a pre-turbulent flow rate of 1.75 mL/min (Re=2360, capillary pressure drop 530 psi) and at a turbulent flow rate of 3.00 mL/min (Re=3930, capillary pressure drop 1750 psi). The retention factor of coronene is close to 0 (same as that of the sample diluent dichloromethane). The retention factor of the impurity was then measured **k**=0.06 which is well smaller than 0.2.

Remarkably and as expected from the chromatograms shown in Figure 1, the unknown sample impurity is initially barely detected and separated from the peak of coronene at a flow rate of 1.75 mL/min (pre-turbulent flow regime). In contrast, at a flow rate of 3.00 mL/min (sustained turbulent flow regime), the impurity peak is almost baseline separated from that of coronene. The retention time of the impurity decreases from 18.3 s to only 10.6 s (speed $\times$ 1.7), the column efficiency increases from 4530 to 32,965 (performance $\times$ 7.3), its peak height increases from 1.7 mAU to 5.7 mAU (sensitivity $\times$ 3.4), and the pressure drop along the OTC increases from 530 to 1750 psi (pressure cost $\times$ 3.3).

5 Conclusion

In this work, the mass transfer mechanisms of small molecules along a 180 μm i.d. $\times$ 20 m long $\times$ 0.2 μm film thickness OTC using pre-turbulent and turbulent mobile phases (carbon dioxide/methanol mixtures) were determined and compared under retained conditions ($0 < \mathbf{k} < 1$). Under pre-turbulent flow regime, the dispersion coefficient of the analytes is around 3×10^{-4} cm^2/s, which is six times as large as their bulk diffusion coefficient. This is explained by the presence of unstable and decaying pre-turbulent puffs generated by the imperfection of the SFC system (injection event, flow delivery of the mobile phase mixture, ABPR ripple). The mass transfer mechanism is still controlled by the slow molecular transport **in the entire volume of the mobile phase despite the presence of vanishing turbulent puffs**. Under sustained turbulent flow regime, the dispersion coefficient of the analyte is about four to five orders of magnitude larger than the bulk diffusion coefficient. Unlike the prediction of the general Golay HETP equation, which anticipates negligible mass transfer resistance in the mobile phase, experiments revealed that the analyte bandspreading is still controlled by the slow mass transfer of the analyte across **the thin viscous layer and the film of stationary phase**. This is directly explained by the presence of the viscous and buffer layers in the wall region region of the OTC. In these layers, which occupy about 30% of the capillary volume at a Reynolds number of 5000, the viscous forces are still dominant over the inertial forces and the molecular transport remains slow.

Similarly to what is observed in a pre-turbulent flow regime, the RPHs recorded at Re=5000 are then increasing from about 5 to 25, 80, and to 110 with increasing the retention factor from 0 to 0.2, 0.5, and to 1.0, respectively. Relative to the RPHs measured under laminar flow at Re =2000, the RPHs measured at Re=5000 are reduced by a factor 9, 5, 3, and 3, respectively. At the same time, the cost in pressure is multiplied by about a factor 4 when doubling the flow rate from laminar to turbulent flow regime.

From a practical viewpoint, the use of carbon dioxide/methanol mixtures as a turbulent mobile phase in OTC can be advantageously used in separation science only and only if the retention factor of the analytes remains smaller than 0.2. Otherwise, the observed gain in peak resolution would be marginal and it would not be worth the cost in system pressure. The proof-of-concept of of

the experimental advantage of turbulent flow chromatography using carbon dioxide as the mobile phase is demonstrated for **k**=0.06. Further experiments are now under investigation regarding ultra-fast chiral SFC separation of non-volatile enantiomers using immobilized cyclodextrin into sol-gels (polymer polyethyleneglycol and crosslinked methyltriethoxysilane) as stable stationary phases [30]. **The estimation of the peak capacity that could be obtained in turbulent flow chromatography using open tubes will then be investigated. Obviously, as shown in this work, turbulent open tube chromatography is not designed to deliver high peak capacity due to the limitation in retention factor ($k^{'}$¡1).**

Finally, from a fundamental viewpoint, the general Golay HETP equation derived for turbulent flow has to be revisited by taking into consideration the known variation of the local dispersion coefficient across the whole i.d. of the capillary column [26]. In a forthcoming investigation, numerical predictions will be performed by considering the general dispersion model of Aris by dispersion (induced by turbulent flow), convection, and distribution between phases (**k** $\neq$0) [2] and compared to the available data. The radial profile of the dispersion coefficient will be extracted from independent and accurate experimental data [26].

6 Acknowledgements

The authors would like to acknowledge and thank Michael Fogwill (Waters, Milford, MA, USA) for fruitful suggestions regarding the design of the instrumentation used in this work.

References

[1] M. J. E. Golay, Theory of chromatography in open and coated tubular columns with round and rectangular cross-sections, In : DH Desty, ed. Gas Chromatography 1958 (Amsterdam symposium), Butterworths, London, pp. 36-55, 1958.

[2] R. Aris, On the dispersion of a solute by diffusion, convection and exchange between phases, Proc. Roy. Soc. A 252 (1959) 538–550.

[3] A. Darbyshire, T. Mullin, Transition to turbulence in constant-mass-flux pipe flow, J. Fluid Mech. 289 (1995) 83–114.

[4] H. Faisst, B. Eckhard, Sensitive dependence on initial conditions in transition to turbulence in pipe flow, J. Fluid Mech. 504 (2004) 343–352.

[5] B. Eckhard, Introduction. turbulence transition in pipe flow: 125th anniversary of the publication of reynolds paper, Philos. Trans. R. Soc. London Ser. A 367 (2009) 449–455.

[6] B. Eckhard, Turbulence transition in pipe flow: some open questions, Nonlinearity 21 (2008) T1–T11.

[7] K. Avila, D. Moxey, A. de Lozar, M. Avila, D. Barkley, B. Hof, The onset of turbulence in pipe flow, Science 333 (2011) 192–1.

[8] L. F. Flint, P. Eisenklam, Longitudinal gas dispersion in transitional and turbulent flow through a straight tube, Canadian Journal of Chemical Engineering 47 (1969) 101–106.

[9] L. F. Flint, P. Eisenklam, Dispersion of matter in transitional flow through straight tubes, Proc. Roy. Soc. Lond. A 315 (1970) 519–533.

[10] J. C. Giddings, W. A. Manwaring, M. N. Myers, Turbulent-gas chromatography, Science 154 (1966) 146–148.

[11] V. Pretorius, T. Smuts, Turbulent flow chromatography. a new approach to faster analysis, Anal. Chem. 38 (1966) 274–281.

[12] R. De Pauw, K. Choikhet, G. Desmet, K. Broeckhoven, Occurrence of turbulent flow conditions in supercritical fluidchromatography, J. Chromatogr. A 1361 (2014) 277–285.

[13] T. Berger, Characterizing pressure issues due to turbulent flow in tubing, inultra-fast chiral supercritical fluid chromatography at up to 580 bar, J. Chromatogr. A 1475 (2016) 86–94.

[14] F. Gritti, M. Fogwill, Molecular dispersion in pre-turbulent and sustained turbulent flow of supercritical carbon dioxide, J. Chromatogr. A 1564 (2018) 176–187.

[15] J. Giddings, Dynamics of Chromatography, Marcel Dekker, New York, NY, 1965.

[16] A. Van Es, J. Rijks, C. Cramers, Turbulent flow in cappilary gas chromatography, J. Chromatogr. 477 (1989) 39–47.

[17] F. Gritti, M. Fogwill, Speed-resolution advantage of turbulent supercritical fluidchromatography in open tubular columns: Ii theoretical andexperimental evidences, J. Chromatogr. A 1501 (2017) 142–150.

[18] R. Tijssen, Axial Dispersion in helically coiled open columns for chromatography, Ph.D. Thesis, Delft University, Delft, pp. 84, 1979.

[19] M. Martin, G. Guiochon, Y. Walbroehl, J. W. Jorgenson, Peak broadening in open-tubular liquid chromatography with electroosmotic flow, Anal. Chem. 57 (1985) 559–561.

[20] F. Gritti, Extension of golay's plate height equation from laminar to turbulent flow i- theory, J. Chromatogr. A 1492 (2017) 129–135.

[21] R. Bird, W. Stewart, E. Lightfoot, Transport Phenomena, John Wiley and Sons, New York, NY, 2002.

[22] D. D. Joseph, B. H. Yang, Friction factor correlations for laminar, transition and turbulent flow in smooth pipes, Physica D 239 (2010) 1318–1328.

[23] C. Colebrook, Turbulent flow in pipes, with particular reference to the transition region between the smooth and rough pipe laws, J. Inst. Civil Eng. 39 (1938) 133–156.

[24] K. Chao, V. Wang, H. Yang, C. Wang, Estimation of effective diffusion coefficients for benzene and toluene in pdms for direct solid phase microextraction, Polymer Testing 30 (2011) 501–508.

[25] C. Wilke, P. Chang, Correlation of diffusion coefficients in dilute solutions, AIChE J. 1 (1955) 264–270.

[26] A. Quarmby, R. K. Anand, Axisymmetric turbulent mass transfer in a circular tube, J. Fluid. Mech. 38 (1969) 4533–455.

[27] B. Poling, J. M. Prausnitz, J. O'Connell, The Properties of Gases and Liquids - Fifth Edition, McGraw-Hill, New York, NY, 2001.

[28] J. Hart, I. Guymer, A. Jones, V. Stovin, Longitudinal Dispersion Coefficients within Turbulent and transitional Pipe Flow, In : P. Rowinski (ed.), Experimental and Computational Solutions of Hydraulic problems, Springer Berlin Heidelberg, London, pp. 133-145, 2013.

[29] K. Ekambara, J. B. Joshi, Axial mixing in pipe flows: turbulent and transition regions, Chem. Eng. Sci. 58 (2003) 2715–2724.

[30] G. Delahousse, V. Peulon-Agasse, J. Debray, M. Vaccaro, G. Cravotto, I. Jabin, P. Cardinael, The incorporation of calix[6]arene and cyclodextrin derivatives intosolgels for the preparation of stationary phases for gaschromatography, J. Chromatogr. A 1318 (2013) 207–216.

Figure captions

Figure 1: Experimental peak profiles of coronene recorded after increasing stepwise the flow rate from 0.5 mL/min to 3.70 mL/min. The capillary dimensions are 180 μm i.d. $\times$ 20 m length $\times$ 0.2 μm film thickness (crosslinked polymethylphenylsiloxane). The mobile phase is mixture of carbon dioxide and methanol (99/1, v/v) and the temperature is set by the lab air-conditionner at 296 $\pm$ 1 K. Coronene is not retained, so, **k**=0. The ABPR pressure is set constant at 1500 psi. Injection volume: 0.4 μL. On capillary detection at L_{corr}=19.6 m. Note the sudden increase in peak height for flow rates larger than 1.75 mL/min indicating a sudden change in the nature of the mass transfer mechanism in the OTC.

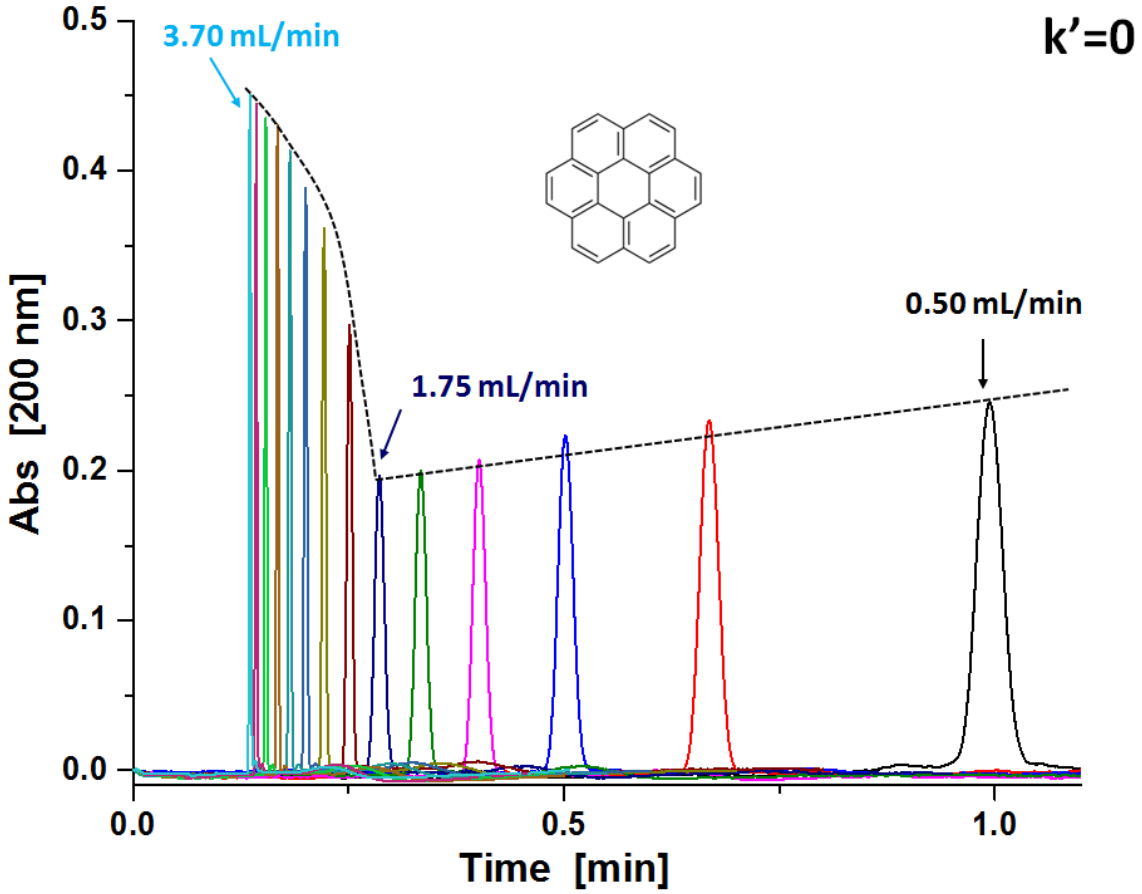

Figure 2: **Same as in Figure 1, except the mobile phase is a mixture of carbon dioxide and methanol (99/2, v/v) and the temperature is adjusted by the GC oven (see details in the experimental section) in order to maintain constant the retention factor at k=0.200 ± 0.012**

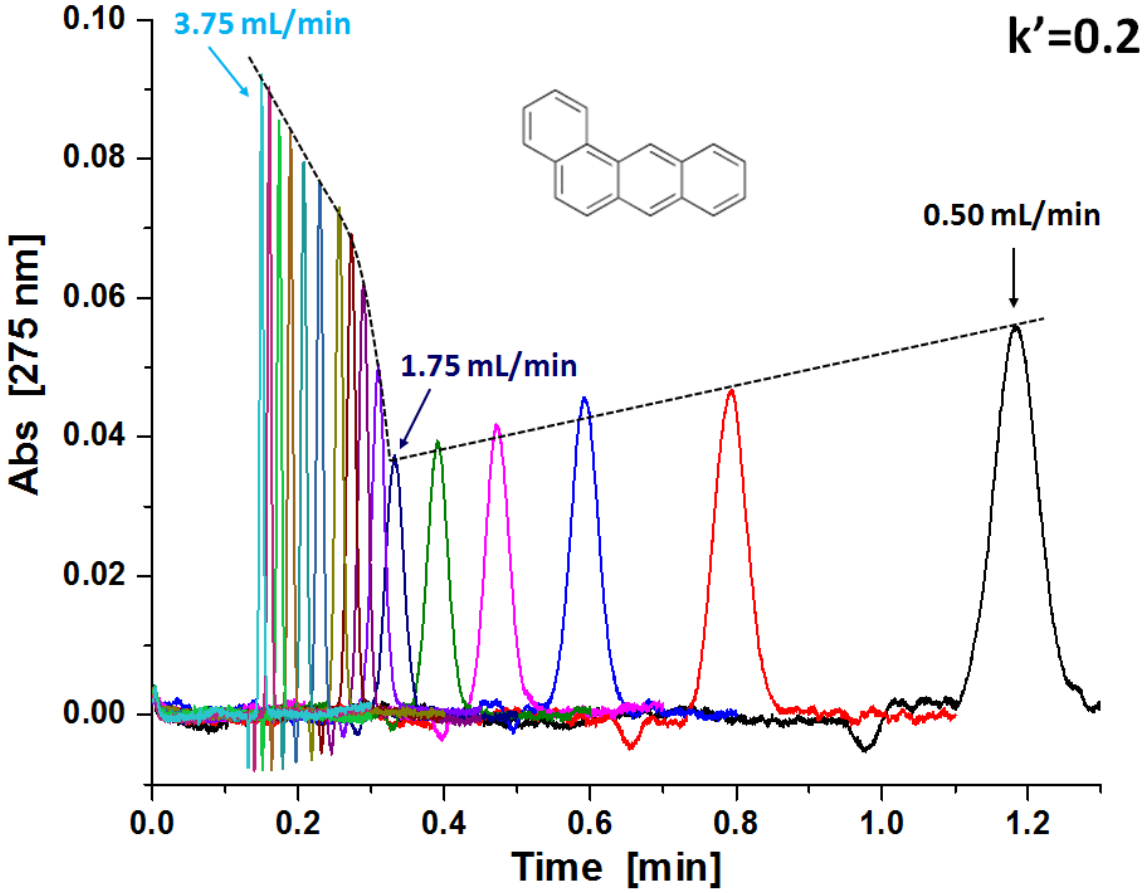

Figure 3: **Same as in Figure 2, except the retention factor is set at k=0.50 ± 0.03 and the sudden increase in peak height for flow rates larger than 1.50 mL/min.**

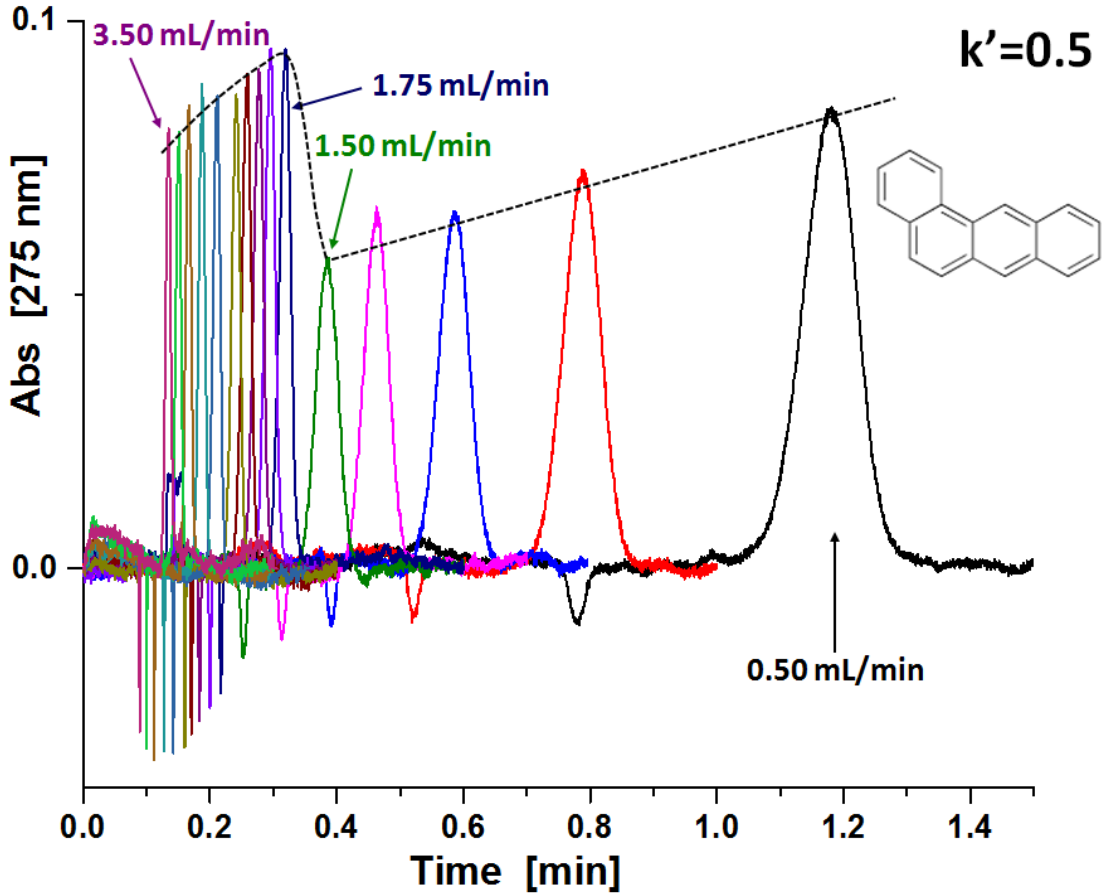

Figure 4: **Same as in Figure 2, except the retention factor is set at k=1.00 ± 0.06 and the sudden increase in peak height for flow rates larger than 1.50 mL/min.**

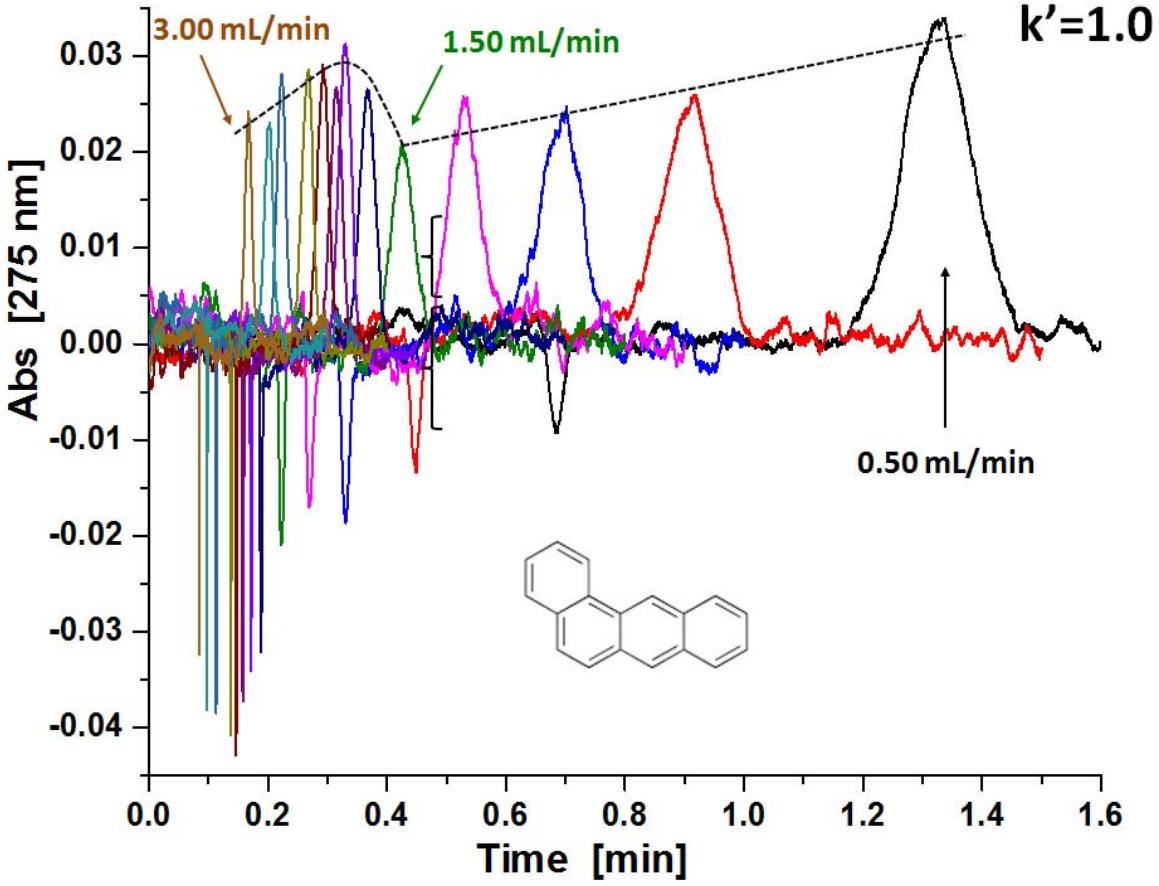

Figure 5: Plot of the experimental RPH of coronene *versus* the Reynolds number (empty green stars). k=0. Same experimental conditions as in Figure 1. For the sake of comparison, the calculated plots of the RPH *versus* the Reynolds number under laminar (Golay Eq. 4 for n=2, full red circles) and turbulent (Golay Eq. 4 for n >2, empty blue circles) flow regimes were added. Note the large discrepancies between the experimental and the calculated RPH plots revealing 1) the existence of turbulent puffs under laminar flow regime and 2) a slow mass transfer in the viscous layer under turbulent flow regime.

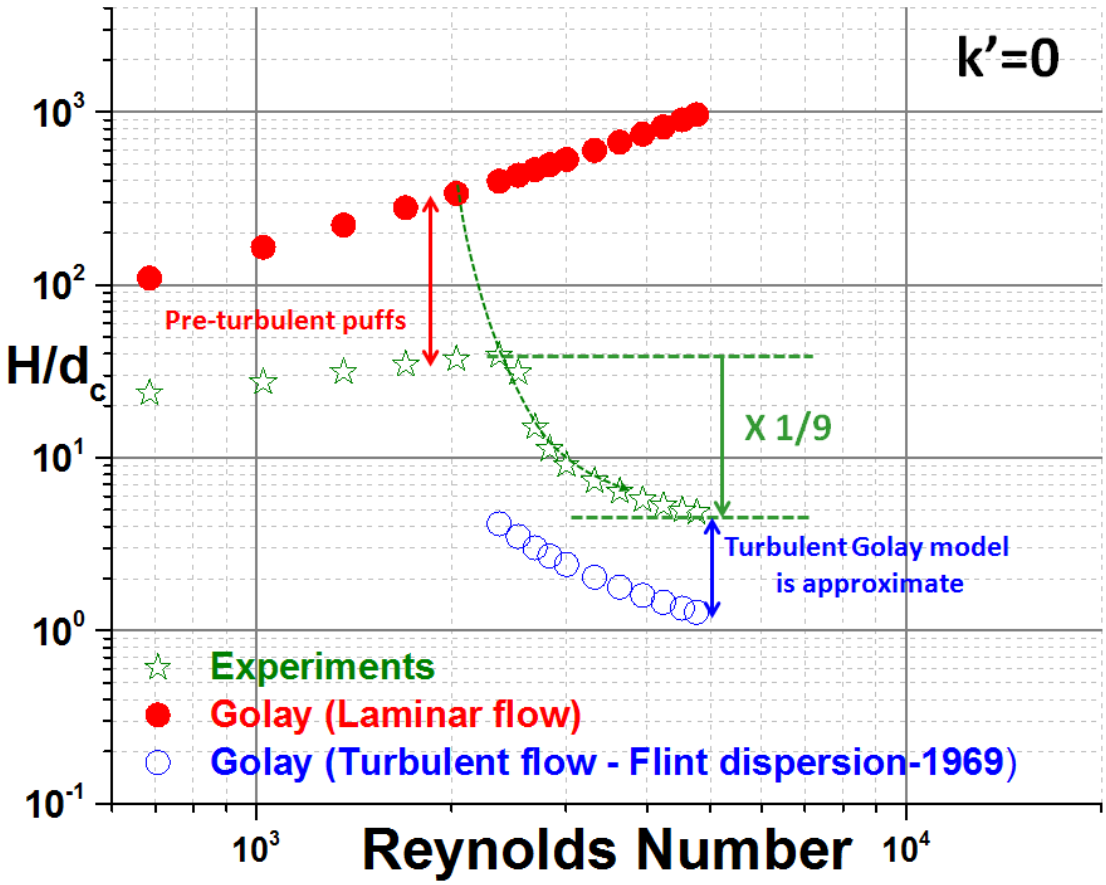

Figure 6: Plot of the experimental RPH of benzo[a]anthracene *versus* Reynolds number (empty green stars). k=0.2. Same experimental conditions as in Figure 2. For the sake of comparison, the calculated plots of the RPH *versus* the Reynolds number under laminar (Golay Eq. 4 for n=2, full red circles) and turbulent (Golay Eq. 4 for n >2, empty blue circles) flow regimes were added.

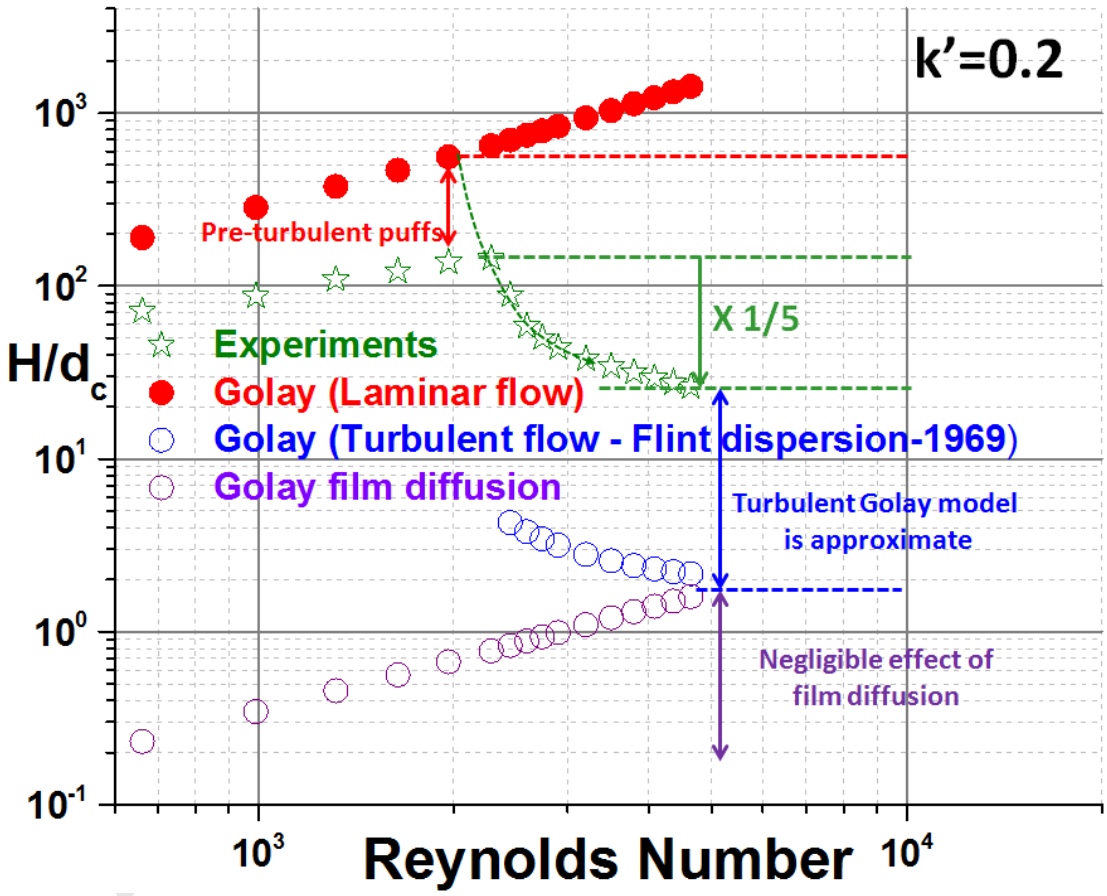

Figure 7: Plot of the experimental RPH of benzo[a]anthracene *versus* Reynolds number (empty green stars). **k**=0.5. Same experimental conditions as in Figure 3. For the sake of comparison, the calculated plots of the RPH *versus* the Reynolds number under laminar (Golay Eq. 4 for n=2, full red circles) and turbulent (Golay Eq. 4 for n >2, empty blue circles) flow regimes were added.

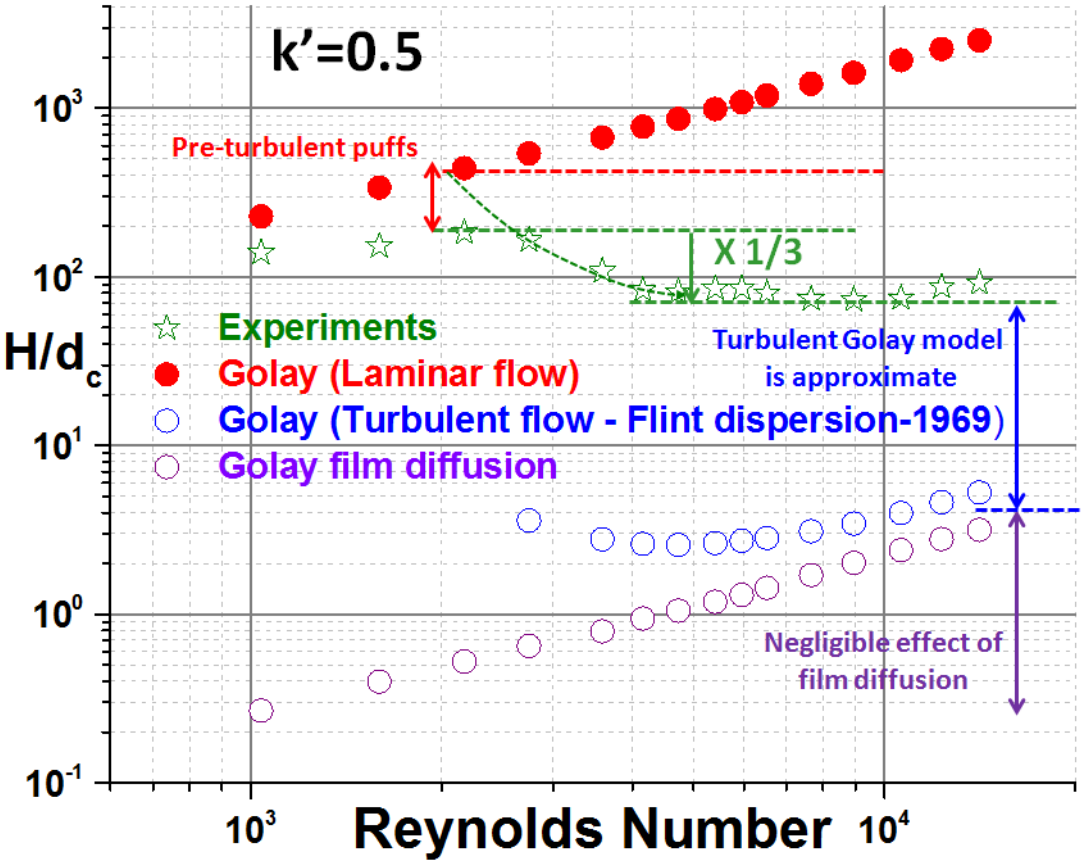

Figure 8: Plot of the experimental RPH of benzo[a]anthracene *versus* Reynolds number (empty green stars). **k**=1.0. Same experimental conditions as in Figure 4. For the sake of comparison, the calculated plots of the RPH *versus* the Reynolds number under laminar (Golay Eq. 4 for n=2, full red circles) and turbulent (Golay Eq. 4 for n >2, empty blue circles) flow regimes were added.

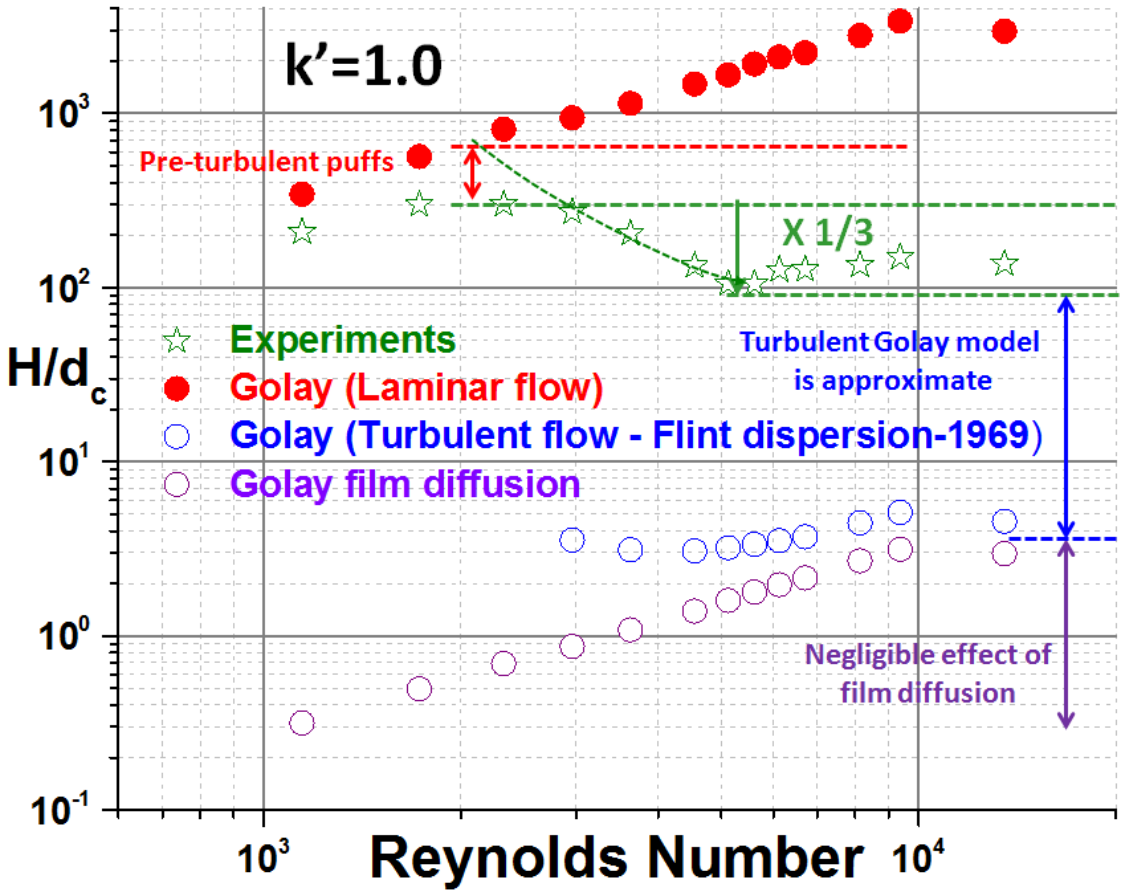

Figure 9: Plot of the semi-empirical average dispersion coefficients, $\overline{D_a}$, of coronene (empty black and red stars for laminar and turbulent flow regimes, respectively) as a function of the Reynolds number. $\overline{D_a}$ is obtained from the best agreement between the experimental RPH data shown in Figure 5 and the general Golay HETP equation Eq. 4. **k**=0. For the sake of comparison, the bulk diffusion coefficients D_m are shown as full black circles and the true turbulent dispersion coefficients from Flint and Eisenklam are represented by the full blue stars.

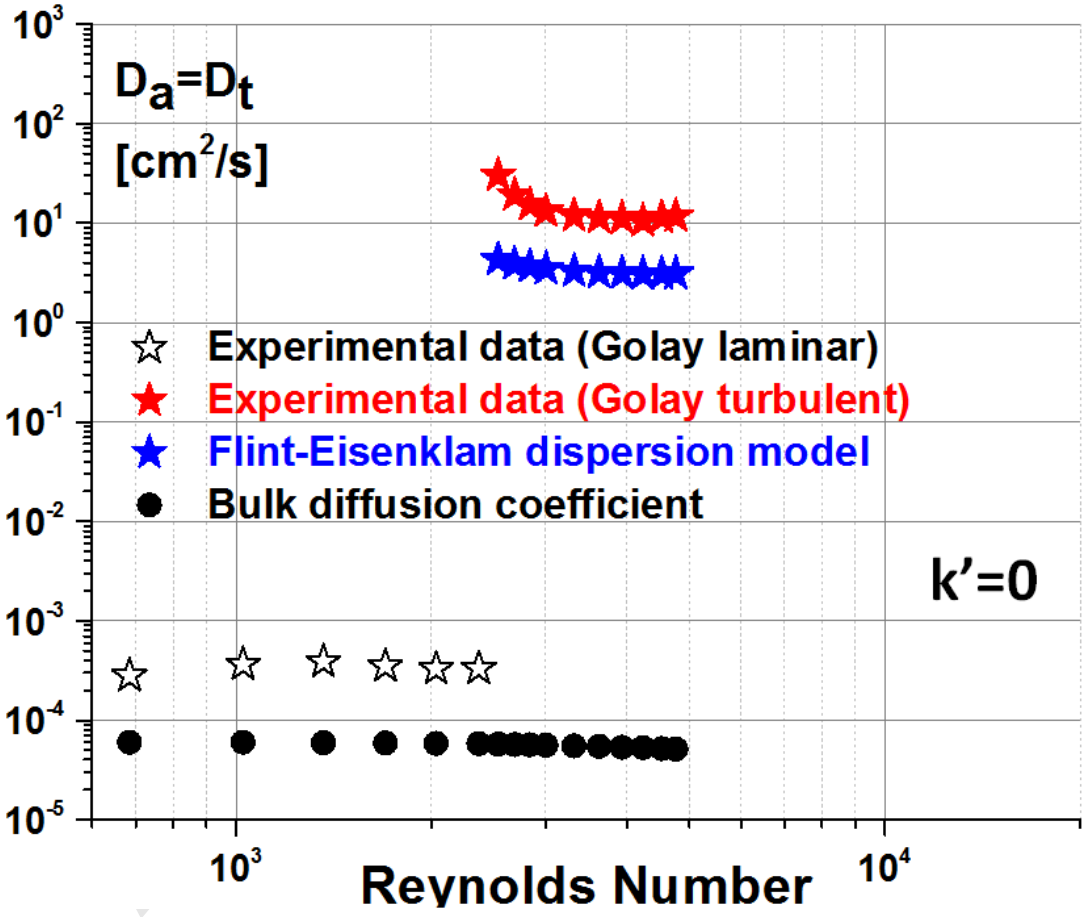

Figure 10: **Same as in Figure 9, except the retention factor is set at k=0.2.**

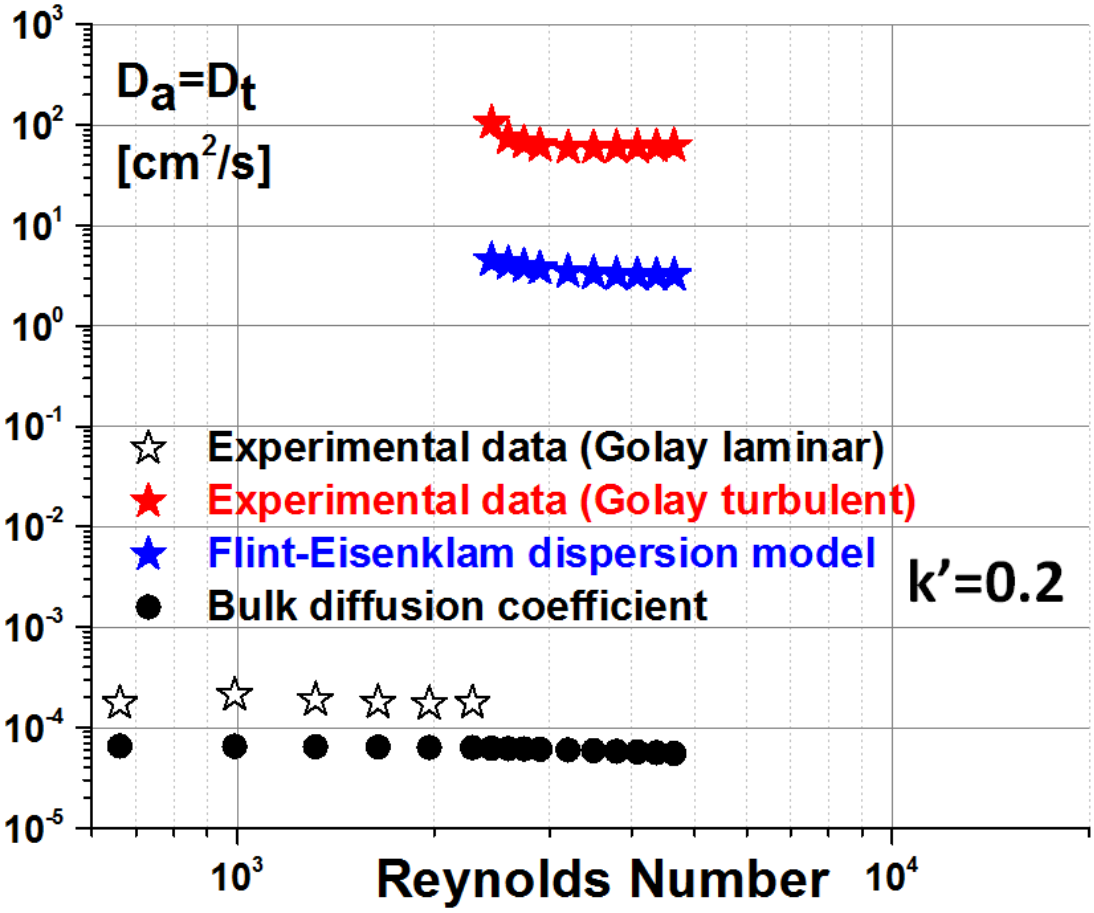

Figure 11: **Same as in Figure 9, except the retention factor is set at k=0.5.**

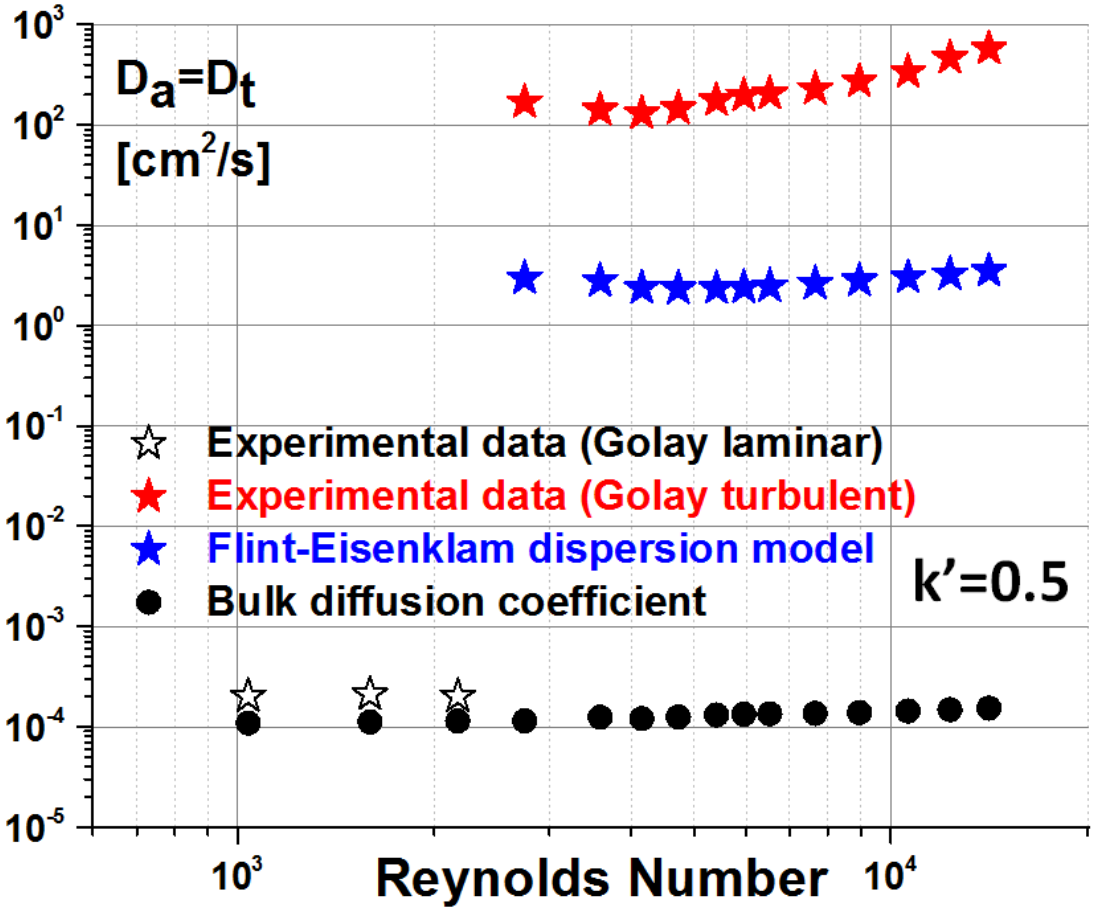

Figure 12: **Same as in Figure 9, except the retention factor is set at k=1.0.**

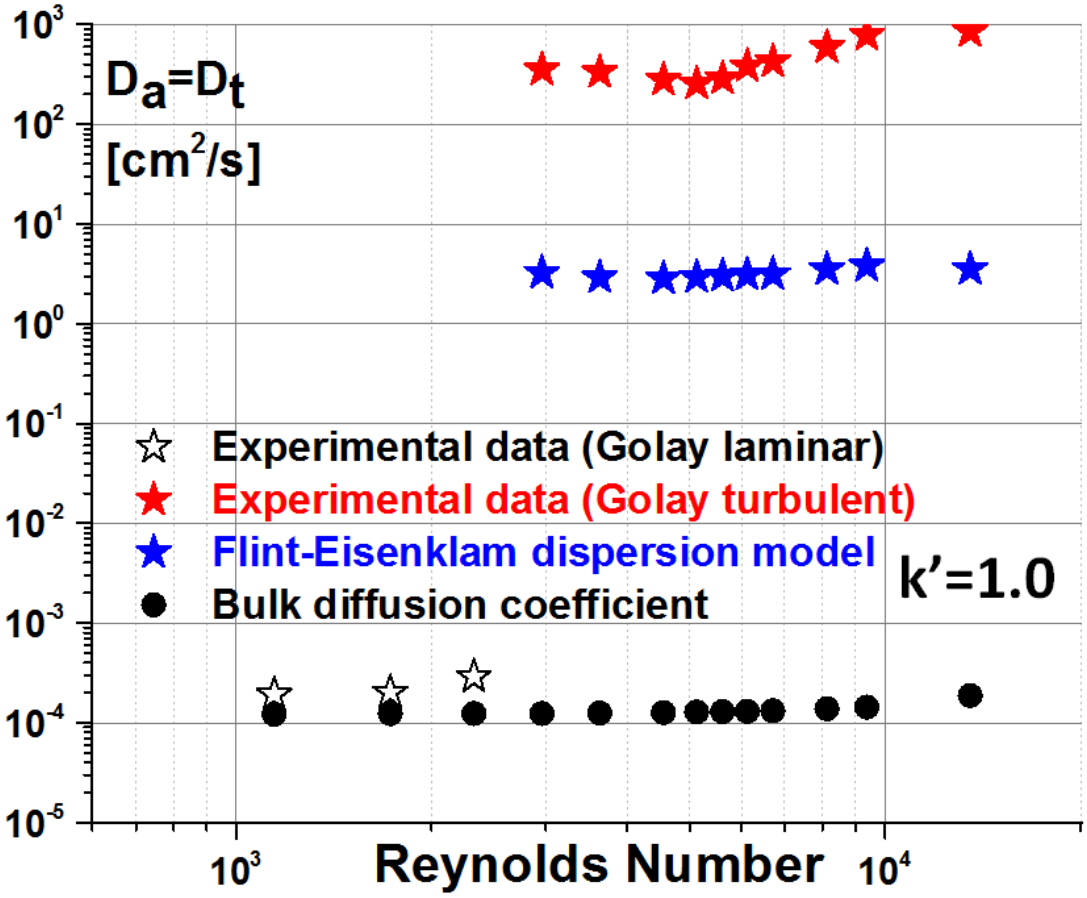

Figure 13: Experimental variation of the local dispersion coefficient, D_a, under turbulent flow regime across pipes for Reynolds numbers increasing from 20800 to 33000, 66900, 81950, 101000, 119100, and to 129900. With permission from J. Fluid Mech. and reference [26]. Note the rapid drop of D_a towards D_m across to the viscous layer and the maximum observed at half the distance between the center and the wall of the pipe in the turbulent bulk layer.

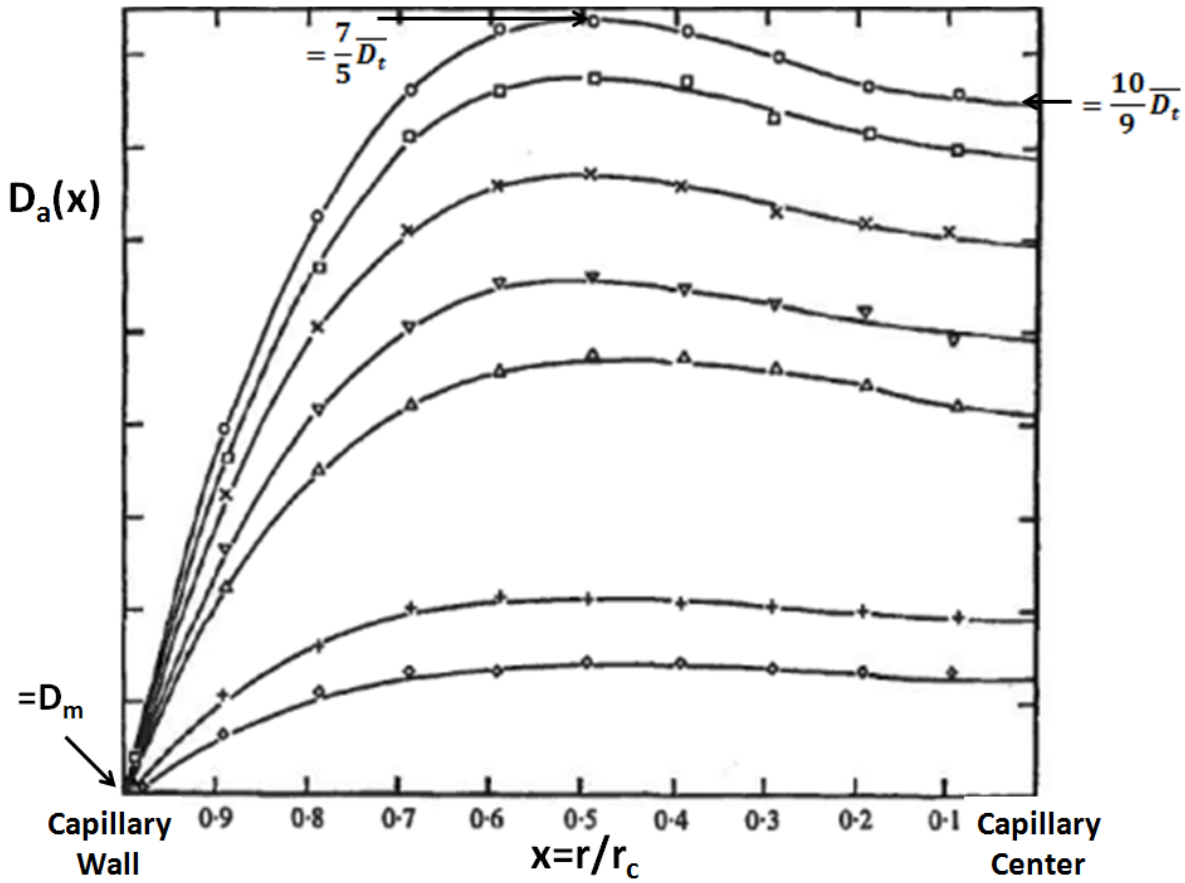

Figure 14: Variation of the expected peak capacity as a function of the retention factor of the last eluted peak under isocratic conditions in turbulent flow chromatography using a 20 m long × 180 μm i.d. open capillary column. The retention factor of the last retained compound increases from 0 to 1. The Reynolds number is set to 5000.

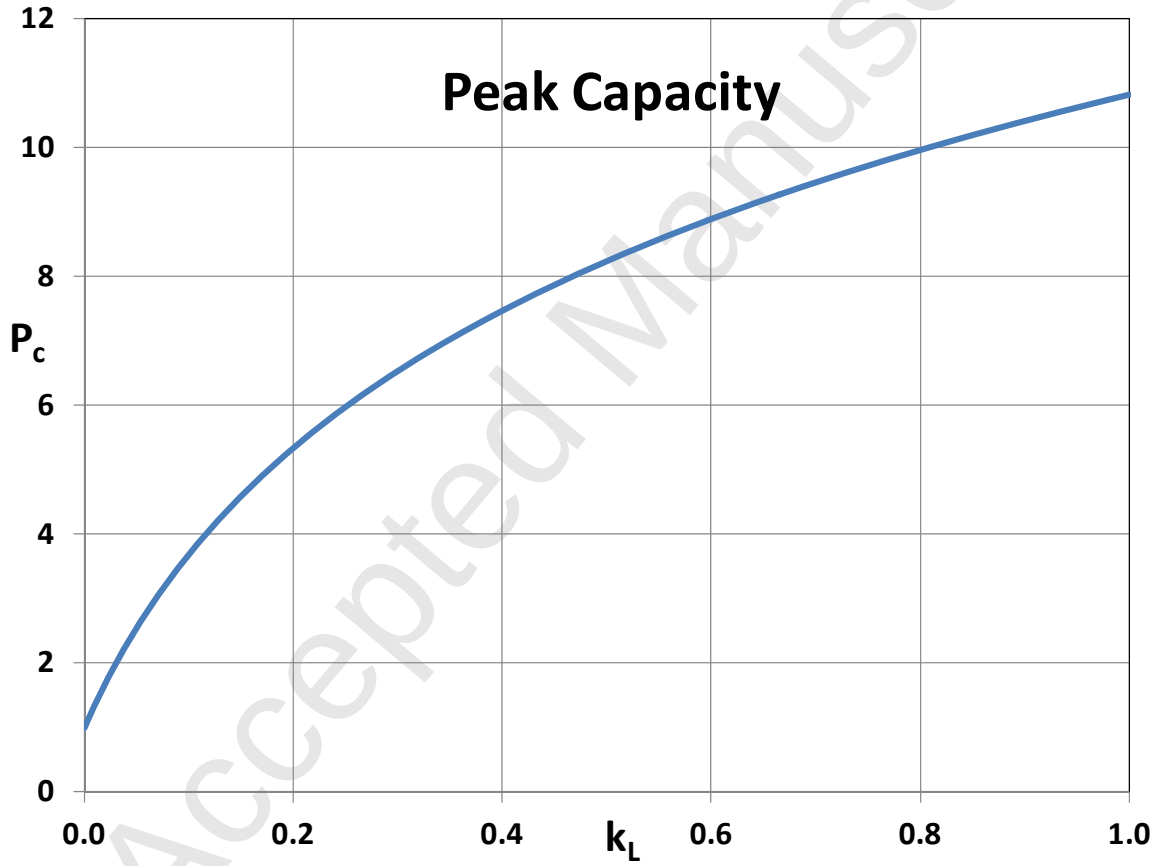

Figure 15: Separation of an unknown impurity (**k**=0.06) in the sample solution of the main component coronene by applying ultra-fast turbulent flow chromatography in open tubular columns. Same experimental conditions as in Figure 1. (Left) Pre-turbulent flow regime (F_v=1.75 mL/min in Figure 1). The impurity is barely visible on the right-hand-side of the main peak of coronene. **For the sake of better visualization, the shaded area was simply drawn and extrapolated from the observed right-hand-side of the impurity signal and from the baseline level.** (Right) Sustained turbulent flow regime (F_v=3.00 mL/min in Figure 1). Relative to classical laminar flow chromatography, the unknown impurity is nearly baseline-resolved (efficiency of 33,000 *vs.* 4,500) while the analysis time is reduced by 45% to only 10 s *vs.* 19 s.